Proceedings of the Combustion Institute 40 (2024) 105330

Contents lists available at ScienceDirect

Proceedings of the Combustion Institute

journal homepage: www.elsevier.com/locate/proci

Predictions of instantaneous temperature fields in jet-in-hot-coflow flames using a multi-scale U-Net model

Jordan A.C. Kildare [a,*], Wai Tong Chung [b], Michael J. Evans [c], Zhao F. Tian [a], Paul R. Medwell [a], Matthias Ihme [b]

[a] School of Electrical and Mechanical Engineering, The University of Adelaide, SA 5005, Australia
[b] Department of Mechanical Engineering, Stanford University, CA 94305, USA
[c] UniSA STEM, The University of South Australia, SA 5095, Australia

ARTICLE INFO

Keywords:
MILD combustion
Jet in hot coflow (JHC)
Machine learning
Temperature prediction

ABSTRACT

A multi-scale U-Net machine learning (ML) model is developed to assess its validity as a surrogate for non-intrusive flame temperature measurement in jet-in-hot-coflow (JHC) flames. Inputs to the model are simultaneous hydroxyl (OH) and formaldehyde (CH_2O) planar laser-induced fluorescence (PLIF) measurements, with target temperature fields derived from Rayleigh scattering measurements. Coflow oxygen (O_2) concentration, jet Reynolds number, coflow temperature, and fuel inputs were considered in the dataset, resulting in 33 unique flame conditions, and ~17,000 training images. The ML model reconstructs the instantaneous temperature images to within an absolute error of 7 ± 10% of the measured values for the initial natural gas/ethylene model. Transfer learning was employed to accelerate training across conditions of different fuels, with mean absolute reconstruction error of 7 ± 9% for models of ethanol and dimethyl ether. A fourth model including data from all four fuels was trained using transfer learning, with 6 ± 9% error. Multi-layer perceptron (MLP) classification models were applied to the deepest layers of the four-fuel model to identify whether physical and chemical flame features were being encoded. Experimentally verifiable features were found to be encoded within the latent space of the model, demonstrating that it is not solely an image regression tool, but is capable of predicting flame features including the fuel type, initial coflow temperature, downstream axial location, and coflow O_2 concentration. These findings indicate that the model is not only well suited for temperature predictions, but can provide scientific insight as well.

1. Introduction

Machine learning (ML) has become prolific in scientific research, capable of solving otherwise intractable problems. Due to the broad scope of ML tools, applications in combustion research vary significantly [1]. In particular, deep learning methods involving convolutional neural networks (CNN) have been used in laser diagnostics measurements via image or spatial field regression. Velocity field predictions with CNNs have been conducted, combining hydroxyl (OH) planar laser induced fluorescence (PLIF) with particle image velocimetry (PIV) to predict velocity fields [2]. One-dimensional spatial fields have also been correlated from experimental data using CNNs, where Raman-Rayleigh scattering and carbon monoxide (CO) LIF are combined to identify combustion regimes with high levels of accuracy [3]. Recently, a CNN has been applied to reconstruct temperature fields using OH-PLIF and soot volume fraction measurements in turbulent toluene diffusion flames in a hot coflow [4]. Only flames at 9% coflow oxygen (O_2) concentration were assessed in that work, using only one fuel [4], limiting the capacity for extension to non-sooting flames, or alternative fuels. Further to the sooting limitation, conditions of 3% O_2 concentration show markedly different flame characteristics from 9% O_2 flames [5,6], requiring further analysis.

To explore the capabilities of ML in temperature predictions over a wider range of flame conditions, further work is needed. Extant temperature measurements that are highly temporally and spatially resolved typically rely on laser diagnostic methods. However, in confined flames and pressurised flames, or apparatus with limited optical accessibility, lased-based temperature measurements are challenging. Under many realistic conditions, laser diagnostic temperature measurements suffer from interference from soot or droplets [7–9], reflections from walls [10,11], or beam-steering effects [7,11,12]. Although significant improvement in capability has been demonstrated [13,14], these remain ongoing challenges.

* Corresponding author.
E-mail address: jordan.kildare@adelaide.edu.au (J.A.C. Kildare).

https://doi.org/10.1016/j.proci.2024.105330
Received 5 December 2023; Accepted 28 May 2024

Table 1
Range of experimental conditions considered in training data. A note here that in the case of ethanol and DME, a carrier gas of nitrogen was used to transport the pre-vapourised fuel at a constant mole ratio.

Fuel	T_{co} (K)	T_{jet} (K)	Coflow O_2 (% vol.)	$\bar{R}e_{jet}$	Axial locations (mm)	Number of data
NG (≥92% CH_4)	1250–1386	305	3–9	1000–10 000	3–51	920
Ethylene	1250–1386	305	3–11	1000–30 000	3–51	4500
Ethanol	1250–1386	413	3–11	10 000	6–51	6500
DME	1250–1386	413	3–9	10 000	6–51	5000

To pave the way for future experiments, this paper will seek to establish the capabilities of ML to reconstruct temperature fields using more robust laser diagnostic techniques, such as OH and formaldehyde (CH_2O) PLIF, which have become ubiquitous for species measurements to determine flame structure. An ML approach offers the ability to augment existing measurements to provide a surrogate for temperature field measurements with similar accuracy to established experimental methods, where they are currently prohibitive. A CNN is developed to assess the feasibility of this task. Measurements of species that are intrinsically temperature dependent (OH and CH_2O) can be inputted into a CNN architecture to extract instantaneous temperature fields.

This paper proposes a deep learning approach for prediction of temperature, and demonstrates its accuracy at predicting a range of ethylene and natural gas (NG) flames in JHC configurations. Using transfer learning, this ML model is then extended to fuels previously unseen by the model (the isomers dimethyl ether (DME) and ethanol), demonstrating the capacity to reconstruct temperature fields from laser measurements over a significant range of conditions by encoding features of the flow physics and chemistry, rather than just regressing the images.

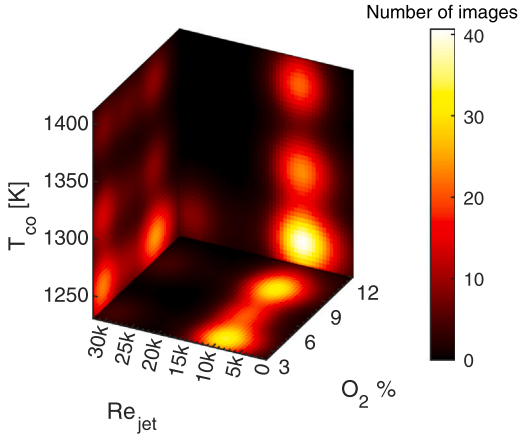

Fig. 1. Projected frequency planes for the experimental condition space. The axes are coflow temperature, Re_{jet}, and coflow O_2 concentration. The planes are coloured by frequency of occurrence.

2. Method and theory

2.1. Experimental data collection

The experimental configuration is a jet-in-hot-coflow (JHC) burner [15,16], with a central turbulent fuel jet (ID = 4.6 mm) issuing into a hot and vitiated laminar coflow (ID = 82 mm). The JHC configuration results in a non-premixed turbulent flame between the cold fuel and hot oxidiser streams. The coflow consists of fuel-lean combustion products from a NG and hydrogen flame, with O_2 concentrations of 3, 6, 9, and 11% (vol/vol). The coflow was controlled by manipulation of the amount of nitrogen present, allowing temperatures to range from 1250–1386 K independent of O_2 concentration. The differences in coflow O_2 level and temperature cause distinctly different behaviour of the reaction zones for similar jet conditions, resulting in diverse flame structures including lifted, attached, and transitional flames [5,15,17]. Variations in the jet Reynolds number (Re_{jet}) also impact the flame structure, as turbulent mixing plays a more significant role compared to molecular diffusion at high Re_{jet} [5].

Simultaneous OH- and CH_2O-PLIF with Rayleigh scattering measurements were recorded, and images of the three scalars were temporally and spatially matched [15,16]. The measurements are statistically stationary, and the images are independent of one another on a shot-to-shot basis. These measurements have previously been presented as quantified and semi-quantified results [15,16], however, the data and methods presented here rely only on the non-quantified intensity images. Table 1 outlines the experimental conditions that were available as the dataset for developing the models, consisting of a total of ~17,000 images across all fuels and conditions. Fig. 1 presents an illustration of the experiment condition space from which the data are drawn, indicating that the majority of data is at Re_{jet} = 10,000, with a coflow temperature of around 1250 K. These data come from images at base heights from 3 mm to 51 mm above the jet exit plane. From these conditions, deterministic random sampling was used to allocate a repeatable portion of the desired input data to training, validation, and testing datasets. Only the training and validation sets are used during the training process to update the model parameters, while the testing set is kept separate, and used only to evaluate the effectiveness of the model. All data presented here is from the testing datasets. The input datasets are split as 80% training, 10% validation, and 10% testing for all models. For the initial model, only ethylene and NG data were used. Ethanol and DME, which are isomers, were incorporated into datasets for transfer learning (refer Section 3.2).

As the proposed model serves as a surrogate for the combustion behaviour of the flames, the use of two separate fuels (NG and ethylene) helps to minimise the amount of training required to encompass other fuels that share similar base chemistry, as in the case of ethanol and DME. Further to the fuel differences, the variation in image heights also helps to generalise the effects of turbulence dominated mixing as opposed to diffusion dominated mixing of the jet and coflow. The differences are particularly relevant in low O_2 flames, where the Damköhler number is on the order of unity.

2.2. ML approach

The CNN architecture used in this work involves a modification of the standard U-Net [18], where the input images are down-scaled and added to each encoding stage to preserve key features. A model architecture diagram can be found in the Supplementary Material S.1. It consists of an input layer, and then four encoding layers, where the latent dimensions are doubled each layer, before reaching the bottleneck layer, the most abstracted layer of the model. Following this layer are four decoding layers, each halving the latent dimensions, before passing through an output layer to reduce dimensions to 1. Compared to other ML approaches, CNNs can be more effective in spatial tasks by extracting spatially dependent relationships through convolution operations. The U-Net is a convolutional autoencoder architecture that transfers information from encoding blocks to decoding blocks at each layer, thus preserving fine-scale features that may otherwise be removed, such as pockets of low temperature due to fuel decomposition in a combusting flow. The resulting model has 25.6 million trainable parameters. This ML model is trained with a mean squared error loss function with

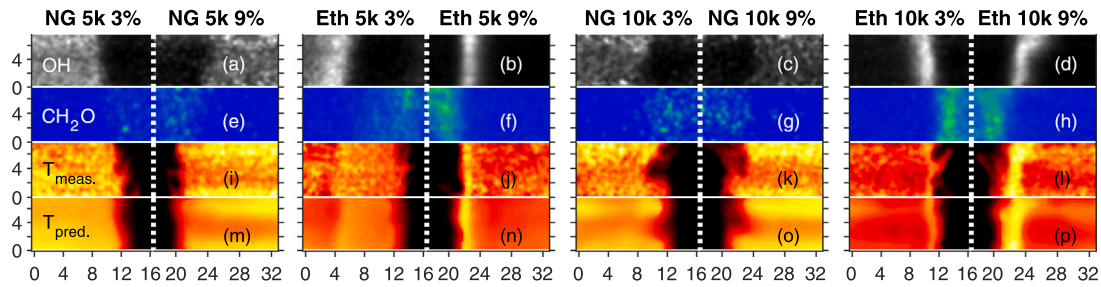

Fig. 2. Example quadruplets of normalised model inputs and outputs for NG and ethylene flames at a bulk mean Re_{jet} = 5000 and Re_{jet} = 10000. The coflow O_2 concentration on each half image is 3% (left), and 9% (right), with an average temperature of 1300 K at the jet exit plane. (a–d) OH-PLIF, (e–h) CH_2O-PLIF, (i–l) Measured Temperature, (m–p) Predicted Temperature. The bottom of each half-image is 23 mm above the jet exit plane. Each half-image is cropped from the original 60 × 8 mm to 16.8 × 7.6 mm for visualisation. The numbered scale is given in millimetres. The vertical dotted lines indicate the jet centreline.

an L2 regularisation term. L2 regularisation penalises large model coefficients, primarily the weights of each neuron, resulting in a more generalised and robust model [19]. Convergence is slower with L2 regularisation, however, the final model tends to be less likely to be over-fitted to the training data.

The U-Net inputs consist of three channels: the OH-PLIF, CH_2O-PLIF images from experiments, and spatial information. Spatial information is modelled as a Gaussian profile, with a mean located at the jet centreline, and a standard deviation of one jet radius, in pixels. This format adds emphasis in the model to the jet centre, where the temperature is vastly different from the coflow, and emphasises the mixing region, where a high temperature gradient exists. Data augmentation is performed by adding random noise to the spatial information [20], which was found to substantially improve model prediction during ML model development. The noise is on the order of 10% of the peak value of Gaussian profile, which is similar to that of the turbulence intensity within the jet, however, significantly higher than that of the coflow. The images are 240 × 32 pixels, with a spatial resolution of ~0.25 mm/pix. The dataset was split through a quasi-random seeded selection, in an 80:10:10 ratio of training, validation and testing data, resulting in approximately 4150 training images, and 520 images for both validation and testing. The model was trained for over 1000 epochs, which was needed for training convergence. The Adam optimiser was employed with an initial learning rate of 10^{-3}, halving every 100 epochs. For transfer learning, the initial learning rate was 10^{-4}.

3. Results and discussion

3.1. Instantaneous temperature field prediction for NG and ethylene flames

Several examples of the model inputs of OH and CH_2O images, along with the target and predicted instantaneous temperature fields are shown in Fig. 2. Cases at Re_{jet} = 5000 and Re_{jet} = 10000 are shown, at coflow O_2 concentrations of 3% and 9% for both NG and ethylene flames. All images are taken at a height of 23 mm above the jet exit, with dimensions of 16.8 × 7.6 mm. Fig. 2 shows an identifiable flame, with distinct zones of high OH, and visible CH_2O that corresponds to some degree with the target peak temperature zones for both ethylene flames at 9% O_2, and for the 3% ethylene flame at Re_{jet} = 10000. No peak temperature zones are observed for the NG cases in Fig. 2, however, there are still distinct regions of OH around the jet-coflow interface, along with breakdown of the fuel into CH_2O in the jet. The differences in species across the presented cases demonstrates the significantly different chemistry and flame structures between ethylene and NG that the model is exposed to.

Images and radial plots of both measured and predicted instantaneous temperatures are shown in Fig. 3 for ethylene and NG flames. Coflow conditions of 3% and 9% O_2 are shown on the left and right of each subplot, respectively. Prediction of the instantaneous temperature fields shows good agreement with the flame shape for both the NG and ethylene flames at the different coflow conditions and heights, although some features of the 3% NG flames downstream are not as well captured. Peak temperature is well predicted, with typical differences on the order of ±5% of the experimental value across all presented conditions. The agreement close to the jet exit and further downstream indicates that the model can adapt to the differences in the turbulent mixing dominated areas as opposed to where the diffusive mixing plays a larger role. In addition, there is reasonable prediction of the temperature field at 25 mm for NG for both 3% and 9% O_2, despite no significant temperature rise to indicate a flame being present. Downstream at 3% O_2, the NG flames show lower quality reconstruction of the turbulent flame structures in the instantaneous measurements. Some of the turbulent structures are not as well predicted, with variation of over 100 K from the measured value. The biasing of the model towards the elevated temperature of the coflow in the NG flames in particular results in this temperature variance, especially when there is a broad OH signal across the coflow. This is a limitation of the model that is alleviated in part through both the multi-scale input at each encoding stage of the U-Net, and through the skip connections in the shallow layers of the U-Net.

Instantaneous temperature fields are well predicted, as are the average fields and the root mean square (RMS) fields. RMS is calculated by averaging the square root of the sum of squared differences between an instantaneous temperature field and the mean field for a given fuel condition. Fig. 4 shows radial plots comparing the average measured and predicted temperatures for several ethylene flames at a coflow temperature of 1250 K and at different Re_{jet}, as well as the RMS of the measured and predicted temperatures. Similar plots for other coflow temperatures are presented in the Supplementary Material S2, with similar accuracy achieved. Prediction of the bulk features of average temperature at different Re_{jet} typically shows peak temperatures matching within 2% of the measured value across the three Re_{jet}. Although there is under-prediction of the RMS fields, the general features are still captured in the predicted flames, highlighting that turbulent structures can be identified with the predicted outputs. The predicted flames are expected to display less variance in the profiles especially in the coflow, due to the inherent smoothing in the convolution process. RMS under-prediction is prevalent in the coflow region particularly, as the length scale of the turbulent structures is similar to the pixel resolution, resulting in a speckled effect that is treated as noise by the model. This is an artefact of the collection resolution, and cannot be avoided. Comparatively, the jet and jet-coflow shear layers display significantly higher RMS, more closely recreating the measured profiles. Overall, the mean absolute reconstruction error was 6.6 ± 9.5% for ethylene, and 7.6 ± 12% for NG.

3.2. Transfer learning to DME and ethanol fuels

Transfer learning is the practice of employing existing model weights that have been previously trained on one ML task, and retraining with small amounts (~10%–20% compared to the original

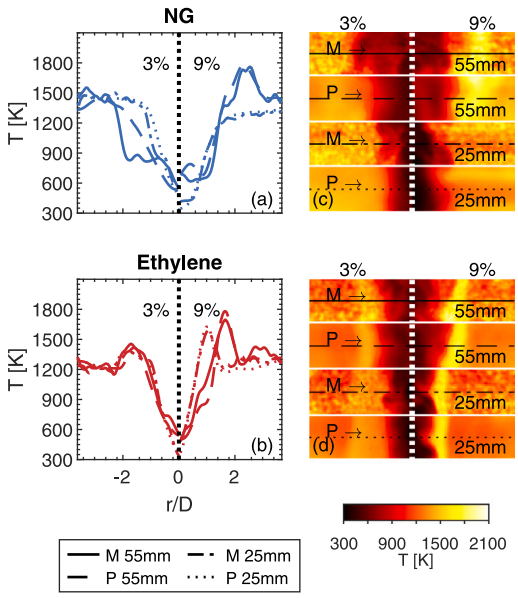

Fig. 3. Instantaneous radial profiles (a–b), and temperature field images (c–d) at 25 mm and 55 mm above the jet exit plane for NG and ethylene flames. Bulk mean jet Re_{jet} = 5000 for all cases, with a coflow O_2 concentration of 3% on the left half of each plot, and 9% on the right half. T_{co} is 1300 K at the jet exit plane. Each half-image is cropped from the original 60 × 8 mm to 16.8 × 7.6 mm for visualisation. Annotations of M and P refer to measured and predicted temperature, respectively. The vertical dotted lines indicate the jet centreline for all plots.

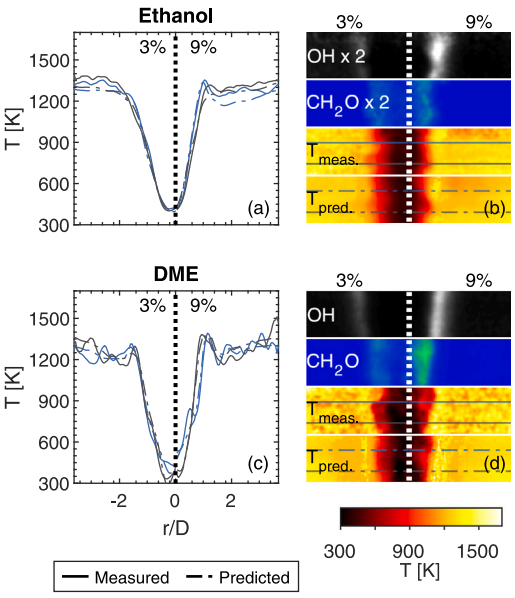

Fig. 5. Instantaneous radial temperature profiles (left) of measured and predicted temperatures, alongside 2D images (right) of measured fields and predicted temperature fields, for (a–b) ethanol, and (c–d) DME. The left half of each subplot is at 3% coflow O_2 concentration, and the right is at 9%. The fuel bulk mean Re_{jet} is approximately 10000 in all cases. The horizontal lines across the 2D temperature images indicate where the radial profiles are extracted. Each half-image is cropped from the original 60 × 8 mm to 16.8 × 7.6 mm for visualisation.

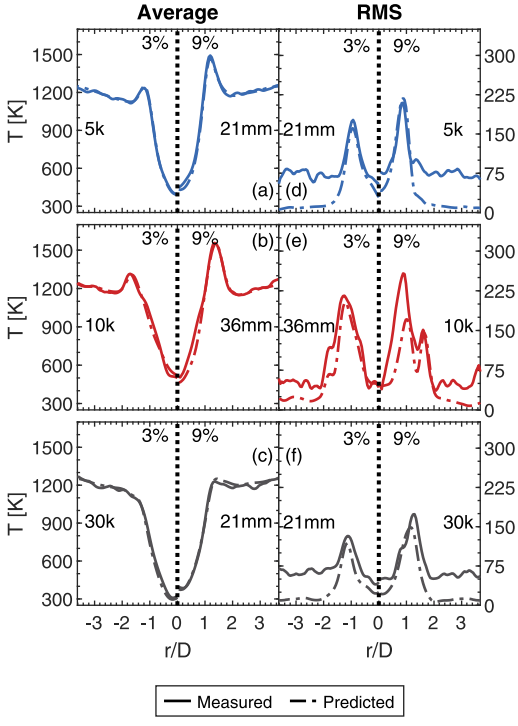

Fig. 4. Radial profiles of average and RMS measured and predicted temperatures for ethylene flames at bulk mean jet Re_{jet} = 5000, Re_{jet} = 10000, and Re_{jet} = 30000, at 25 mm above the jet exit plane, and with a coflow temperature of 1250 K. For each plot, the left side indicates 3% coflow O_2, and 9% on the right. (a–c) Average temperatures profiles, (d–f) RMS temperature profiles.

model) of data for a different ML task [21]. This principle allows rapid adaptation of a model to previously unseen data that typically does not lie within the bounds of what the model has previously encountered, with greater computational and data efficiency. An appropriate use for this technique in the context of temperature prediction is exposure to different fuel types. Transfer learning is applied by freezing the deep layers of the model (80% of the parameters) and only retraining 20% of the model parameters from temperature predictions of ethylene and NG flames with data from ethanol or DME measurements. Here, 20% of number of original training data images per fuel are used as inputs.

Fig. 5 shows radial profiles and 2D images of instantaneous flame temperatures for ethanol and DME after the transfer learning process at a height of 23 mm above the jet exit plane, and two coflow O_2 levels. Normalised OH and CH_2O fields are also shown to highlight differences in the fuels. Overall, the mean absolute error in the prediction for the test set of these flames after transfer learning is 4.2 ± 6.5% for ethanol, and 6.4±8.9% for DME, compared to 13 ± 19% and 11 ± 15% before transfer learning. The new error margin lies within the experimental measurement uncertainty, indicating that the transfer learning approach yields accurate results. Although some of the fluctuations in the temperature field are not as well recreated, the peak temperatures and mixing zones for both ethanol and DME are. The measured instantaneous temperature fields for both ethanol and DME show mixing between the jet-coflow interface resulting in asymmetric profiles that are recreated well with the model predictions. Despite being isomers of one another, DME appears to have a higher peak temperature than ethanol in the jet-coflow mixing region. This property is noted in both the measured and predicted fields, and is consistent with previous experimental observations of these fuels [15,22].

Fig. 5 shows that production of both OH and CH_2O are significantly greater in DME than in ethanol, with at least a two-fold increase in signal at the same coflow and jet conditions. A combination of elevated OH and CH_2O is indicative of high heat release, which is supported by the higher peak temperatures observed for DME when compared with ethanol. Structurally, however, both fuels show a central zone with no decomposition to CH_2O, surrounded by a decomposition zone, which in turn is surrounded by a region of OH. Despite DME and ethanol showing similar OH and CH_2O fluorescence at 3% coflow O_2, the temperature rise at the jet-coflow boundary is sharper for DME,

Table 2
Statistics for the structural similarity index measure (SSIM) for flame temperature field recreation based on the amount of training data as a percentage of the original model training data set. Minimum and maximum SSIM are shown, as are the mean SSIM and standard deviation.

Data (%)	Min	Max	μ	σ	μ/σ
0	0.454	0.698	0.592	0.0534	11.1
5	0.387	0.704	0.611	0.0661	9.24
10	0.409	0.713	0.627	0.0648	9.68
15	0.439	0.711	0.633	0.0614	10.3
20	0.457	0.718	0.643	0.0567	11.3
25	0.466	0.720	0.646	0.0549	11.8
30	0.470	0.722	0.647	0.0545	11.9

peaking above the coflow temperature. The sharp rise in temperature for DME indicates a strong reaction zone which is not observed for ethanol, where the transition is more gradual. The differences observed at 3% O_2 are similar to those discussed regarding the structure of ethanol and DME flames in previous work [15].

The effectiveness of the transfer learning approach was further assessed. To this end, training data volumes of 5% to 30% of the original dataset were used to train different models for DME, and the outputs were tested against a subset of data not seen by any of the models to determine minimum required data volume to achieve accurate results. A separate parameter study investigating the effect of the number of frozen parameters is summarised in the Supplementary Material §3. Table 2 presents statistics for the structural similarity index measure (SSIM) for each proportion of training data provided to train the transfer learning model after convergence is achieved. SSIM is a typical measure of visual perception of whether two images look the same, and is often used in computer vision tasks [23]. The index is maximised at unity when there is perfect recreation, and can be negative if the recreation is extremely poor. Much of the deviation from unity in the SSIM values in Table 2 is due to the smoothing of the coflow noise, however, the trend is clear. Increases in data volume result in a narrowing of the spread of SSIM values, with increases in both the minimum and maximum values. Improvements are noted until a proportion of 20% is reached, which is consistent with typical values for transfer learning effectiveness. However, as little as 10% is a significant improvement over 5% data input, highlighting the importance of training data volume in the transfer learning approach. Interestingly, the untrained original model displays a higher mean to standard deviation ratio of SSIM compared to transfer volumes of less than 20%. However, the mean SSIM performance is less than the 5% data case, and a maximum SSIM also less than the 5% case. This is suggestive of good generalisation of the chemistry from the model, although indicates limitations in detailed recreation quality.

3.3. Investigating model interpretability

To examine whether deep learning approaches can distinguish and understand the underlying physics and chemistry resulting in different temperature fields between different fuels, the hidden layers are investigated, specifically the bottleneck of the U-Net autoencoder. The examination is performed on a new model trained with data from all four fuels. At the bottleneck of this model, the data is encoded into the most latent feature maps. In order to visualise these high-dimensional ($15 \times 2 \times 1024$) bottleneck outputs, principal component analysis (PCA) is employed to reduce the dimensions of these encoded features. Fig. 6 shows a scatter plot of the first two principal components (PCs) of the latent space across the test data set. The different coloured clusters indicate different fuels, and demonstrate the unique latent representation of each fuel. An analysis of the pathway of OH and CH_2O inputs via dummy inputs indicates that PC_1 is strongly dominated in the positive direction by a high CH_2O signal, whilst OH dominates much of PC_2, with a negative trajectory in PC_1.

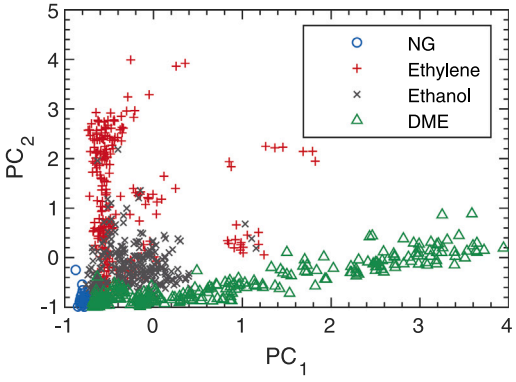

Fig. 6. Scatter plot of the first two PCs of the bottleneck layer of the U-Net. The points are coloured by fuel. (For interpretation of the references to colour in this figure legend, the reader is referred to the web version of this article.)

NG shows the least spread in Fig. 6, primarily due to the lack of variation in temperature conditions observed for most of the training data, as well as weak OH and CH_2O signals. Comparatively, ethylene shows little variation in the first principal component, but significant variation in the second principal component, likely due to the characteristic peak OH zone observed for the majority of experimental flame conditions. Two transitional branches are noted though, where an increase in CH_2O shifts the position of PC_1 positively. This feature is not shared with the other fuels. Comparatively, DME displays significant variation only in the first principal component, with a narrow range in the second component. DME has been shown to have significant CH_2O signals compared to other C_2 fuels [15], contributing to this distribution. DME's isomer, ethanol, displays markedly tighter grouping around the origin of both component axes when compared with DME, owing to the similar scales of OH and CH_2O observed.

Investigating the fuel clusters themselves, flame conditions can be assessed. A multi-layer perceptron (MLP) classifier was trained using the first four components from PCA to extract physical features of the flames, including image height, O_2 concentration, Re_{jet}, and coflow temperature. Four components are required to encompass more than 85% of the variance in the data, essentially preserved 85% of the original un-encoded data. MLPs are typically used in canonical classification problems due to their simplicity and speed. Fig. 7 presents the results of the classifier predictions for fuel type from the full dataset, then image height, O_2 concentration, and coflow temperature on a fuel-by-fuel basis. NG has been omitted in Fig. 7(b–d) due to the small volume of available data, and the Re_{jet} outputs are not shown as both DME and ethanol are at constant Re_{jet}. The performance of each model is summarised in Table 3.

Fig. 7(a) and Table 3 show that fuel species prediction is almost 100% accurate, suggesting that the latent space has fuel-specific features that can be readily identified. In Fig. 7(b), the coflow temperature is well classified for ethylene in particular, with 100% accuracy, although the "All" fuels dataset is well characterised too (>90% accuracy). The implication is that coflow temperature plays a more significant role on the flame features of the ethylene flames, as opposed to the DME and ethanol flames, which has been experimentally observed previously [5,16]. A similar observation is also noted for Fig. 7(d), where oxygen concentration is well predicted particularly for the ethylene and DME cases when compared to classification of ethanol. Image height departs from the trends for ethylene, with both ethanol and DME being classified at different heights to 100% accuracy, as opposed to 71% for ethylene. This suggests that the coflow temperature and oxygen concentration plays a more significant role in flame features than the downstream mixing and fuel jet heating compared to ethanol and DME. Comparing the findings in Fig. 7 to the trends of PC_1 and PC_2 in Fig. 6 indicates that the role of fuel decomposition into CH_2O

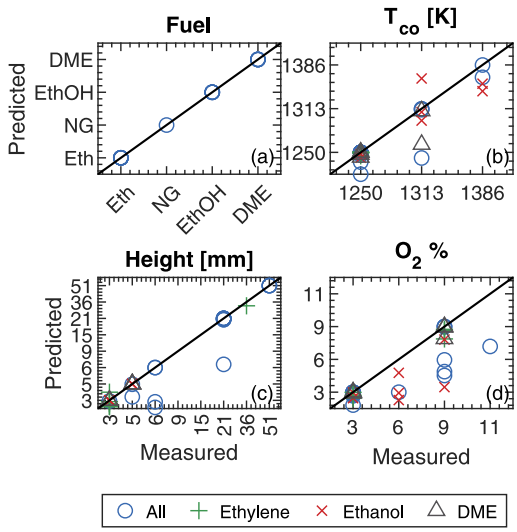

Fig. 7. Scatter plots showing the performance of the classifier outputs from bottleneck of ML model. The diagonal line indicates perfect correlation. Only every fifth point is shown for clarity. (a) Fuel, (b) Coflow temperature, (c) Image height above the burner, (d) Coflow O_2 concentration.

Table 3
Testing scores as a percentage for MLP classifiers for fuel species, coflow temperature, Re_{jet}, coflow O_2 concentration, and image height above the burner.

Dataset	Fuel	T_{co}	Re_{jet}	O_2 %	Height
All	99	91	98	76	93
Ethylene	–	100	89	93	71
Ethanol	–	91	–	67	100
DME	–	90	–	93	100

on key flame features observed in experiments [15] is encoded in the bottleneck. The results from the classifier process indicate that through OH and CH_2O alone, fundamental and distinct differences in the behaviour of different fuels under MILD conditions can be identified by where the classification process is most accurate.

4. Conclusions

A multi-scale U-Net was developed to assess its feasibility as a surrogate for non-intrusive measurement of instantaneous flame temperatures. A wide range of experimental data from a JHC burner was used to train the model in several stages. OH- and CH_2O-PLIF data from 33 unique flame conditions were used in this work, with target temperature fields derived from Rayleigh scattering measurements.

The model demonstrated good overall accuracy in reconstruction of temperature fields from the initial two-fuel model, with errors typically lying within the bounds of the experimental measurement error. Evaluation of the mean and RMS temperature fields also demonstrated a high correlation between the measured and predicted values. A transfer learning approach was implemented to train against ethanol and DME flames, with a data volume assessment demonstrating high reconstruction accuracy (~6% mean absolute error) using only 20% of the original data volume for the ethylene and NG flames.

A separate model was trained through transfer learning using all four fuels. An MLP classifier was applied to the bottleneck layer of the model to identify flame features. The model is capable of identifying the fuel species, and correlations for different fuels with coflow O_2, coflow temperature, and downstream location that provide insight into the flame structure to support previous findings, as well as highlight where there are likely to be fundamental differences in flame structure due to different experimental conditions. In particular, precursor development from the decomposition of DME and ethanol play a major role in the flame structure compared to the coflow O_2 level, whilst coflow temperature and O_2 play a significant role for ethylene.

The four-fuel model highlights both the efficacy of ML to act as a surrogate for non-intrusive temperature measurements, and the ability of the model to encode into the latent space unique, experimentally identifiable features of the flame from only normalised OH- and CH_2O-PLIF data. The implication from these findings is that ML can be reliably used for temperature prediction from OH- and CH_2O-PLIF in experimental conditions that inhibit scattering measurements, serving as a first-order model due to the encoded physics and chemistry of the model.

Novelty and Significance Statement

The novelty of this research is in the prediction of instantaneous temperature fields across a significant range of conditions using a model that is capable of identifying unique and experimentally verifiable flame features in its latent space. It is significant because it demonstrates the ability for machine learning to act as a surrogate for temperature prediction by encoding features of the flames from only normalised intensity images of hydroxyl (OH) and formaldehyde (CH_2O) intensity, rather than simply solving an image regression problem.

CRediT authorship contribution statement

Jordan A.C. Kildare: Co-designed research concept, Planned modelling approach, Analysed data, Interpreted data, Wrote original manuscript. **Wai Tong Chung:** Co-designed research concept, Planned modelling approach, Interpreted data, Edited manuscript. **Michael J. Evans:** Co-designed research concept, Co-acquired experimental data, Interpreted data, Edited manuscript. **Zhao F. Tian:** Co-designed research concept, Interpreted data, Edited manuscript. **Paul R. Medwell:** Co-designed research concept, Co-acquired experimental data, Interpreted data, Edited manuscript. **Matthias Ihme:** Co-designed research concept, Planned modelling approach, Interpreted data, Edited manuscript.

Declaration of competing interest

The authors declare that they have no known competing financial interests or personal relationships that could have appeared to influence the work reported in this paper.

Acknowledgments

The authors acknowledge the generous support of The University of Adelaide, the Australian Research Council (ARC), the United States Asian Office for Research and Development (AOARD), the Australian Government Research Training Program Stipend (RTPS), and supercomputing resources provided by Phoenix HPC at The University of Adelaide. Wai Tong Chung is grateful for financial support from the U.S. Department of Energy, National Nuclear Security Administration under award No. DE-NA0003968. Matthias Ihme acknowledges the support from the U.S. Department of Energy award BE-S0022222.

Appendix A. Supplementary data

Supplementary material related to this article can be found online at https://doi.org/10.1016/j.proci.2024.105330.

References

[1] M. Ihme, W.T. Chung, A.A. Mishra, Combustion machine learning: Principles, progress and prospects, Prog. Energy Combust. Sci. 91 (2022) 101010.

[2] S. Barwey, M. Hassanaly, V. Raman, A. Steinberg, Using machine learning to construct velocity fields from OH-PLIF images, Combust. Sci. Technol. 194 (1) (2022) 93–116.

[3] K. Wan, S. Hartl, L. Vervisch, P. Domingo, R.S. Barlow, C. Hasse, Combustion regime identification from machine learning trained by Raman/Rayleigh line measurements, Combust. Flame 219 (2020) 268–274.

[4] X. Nie, W. Zhang, X. Dong, P.R. Medwell, G.J. Nathan, Z. Sun, Reconstructing temperature fields from OH distribution and soot volume fraction in turbulent flames using an artificial neural network, Combust. Flame 259 (2024) 113182, http://dx.doi.org/10.1016/j.combustflame.2023.113182.

[5] P.R. Medwell, P.A. Kalt, B.B. Dally, Imaging of diluted turbulent ethylene flames stabilized on a Jet in Hot Coflow (JHC) burner, Combust. Flame 152 (2008) 100–113.

[6] M. Evans, A. Chinnici, P. Medwell, J. Ye, Ignition features of methane and ethylene fuel-blends in hot and diluted coflows, Fuel 203 (2017) 279–289.

[7] A.C. Eckbreth, Laser Diagnostics for Combustion Temperature and Species, first ed., CRC Press, 1996.

[8] S.P. Kearney, R.W. Schefer, S.J. Beresh, T.W. Grasser, Temperature imaging in nonpremixed flames by joint filtered Rayleigh and Raman scattering, Appl. Opt. 44 (9) (2005) 1548–1558.

[9] P.R. Medwell, A.R. Masri, P.X. Pham, B.B. Dally, G.J. Nathan, Temperature imaging of turbulent dilute spray flames using two-line atomic fluorescence, Exp. Fluids 55 (11) (2014) 1840.

[10] O. Lammel, M. Stöhr, P. Kutne, C. Dem, W. Meier, M. Aigner, Experimental analysis of confined jet flames by laser measurement techniques, J. Eng. Gas Turbines Power 134 (4) (2012) 041506, http://dx.doi.org/10.1115/1.4004733.

[11] A. Dreizler, B. Böhm, Advanced laser diagnostics for an improved understanding of premixed flame-wall interactions, Proc. Combust. Inst. 35 (1) (2015) 37–64.

[12] S. Kruse, P. Medwell, J. Beeckmann, H. Pitsch, The significance of beam steering on laser-induced incandescence measurements in laminar counterflow flames, Appl. Phys. B 124 (2018) 1–11.

[13] M. Aldén, Spatially and temporally resolved laser/optical diagnostics of combustion processes: From fundamentals to practical applications, Proc. Combust. Inst. 39 (1) (2023) 1185–1228.

[14] G. Nathan, P. Kalt, Z. Alwahabi, B. Dally, P. Medwell, Q. Chan, Recent advances in the measurement of strongly radiating, turbulent reacting flows, Prog. Energy Combust. Sci. 38 (1) (2012) 41–61.

[15] J. Ye, P.R. Medwell, K. Kleinheinz, M.J. Evans, B.B. Dally, H.G. Pitsch, Structural differences of ethanol and DME jet flames in a hot diluted coflow, Combust. Flame 192 (2018) 473–494.

[16] I.J. Shaw, M.J. Evans, R. Chin, P.R. Medwell, Characterisation of ethylene flames under a range of low-oxygen concentrations, Fuel 334 (2023) 126495.

[17] E. Oldenhof, M. Tummers, E. Van Veen, D. Roekaerts, Ignition kernel formation and lift-off behaviour of jet-in-hot-coflow flames, Combust. Flame 157 (2010) 1167–1178.

[18] O. Ronneberger, P. Fischer, T. Brox, U-Net: Convolutional networks for biomedical image segmentation, in: N. Navab, J. Hornegger, W.M. Wells, A.F. Frangi (Eds.), Proc. Med. Image Comput. Comput.-Assist. Interv., 2015, pp. 234–241.

[19] C. Cortes, M. Mohri, A. Rostamizadeh, L2 regularization for learning kernels, 2012, arXiv preprint arXiv:1205.2653.

[20] W.T. Chung, K.S. Jung, J.H. Chen, M. Ihme, BLASTNet: A call for community-involved big data in combustion machine learning, Appl. Energy Combust. Sci. 12 (2022) 100087.

[21] S. Thrun, Lifelong learning algorithms, in: S. Thrun, L. Pratt (Eds.), Learning to Learn, Springer US, Boston, MA, 1998, pp. 181–209.

[22] F. Herrmann, B. Jochim, P. Oßwald, L. Cai, H. Pitsch, K. Kohse-Höinghaus, Experimental and numerical low-temperature oxidation study of ethanol and dimethyl ether, Combust. Flame 161 (2) (2014) 384–397.

[23] Z. Wang, A.C. Bovik, H.R. Sheikh, E.P. Simoncelli, Image quality assessment: from error visibility to structural similarity, IEEE Trans. Image Process. 13 (4) (2004) 600–612.